NANO LETTERS

pubs.acs.org/NanoLett Letter

Theory of Excitons in Gated Bilayer Graphene Quantum Dots

Yasser Saleem,* Katarzyna Sadecka, Marek Korkusinski, Daniel Miravet, Amintor Dusko, and Pawel Hawrylak

Cite This: *Nano Lett.* 2023, 23, 2998−3004 Read Online

ACCESS | Metrics & More | Article Recommendations | Supporting Information

ABSTRACT: We present a theory of excitons in gated bilayer graphene (BLG) quantum dots (QDs). Electrical gating of BLG opens an energy gap, turning this material into an electrically tunable semiconductor. Unlike in laterally gated semiconductor QDs, where electrons are attracted and holes repelled, we show here that lateral structuring of metallic gates results in a gated lateral QD confining both electrons and holes. Using an accurate atomistic approach and exact diagonalization tools, we describe strongly interacting electrons and holes forming an electrically tunable exciton. We find these excitons to be different from those found in semiconductor QDs and nanocrystals, with exciton energy tunable by voltage from the terahertz to far infrared (FIR) range. The conservation of spin, valley, and orbital angular momentum results in an exciton fine structure with a band of dark low-energy states, making this system a promising candidate for storage, detection and emission of photons in the terahertz range.

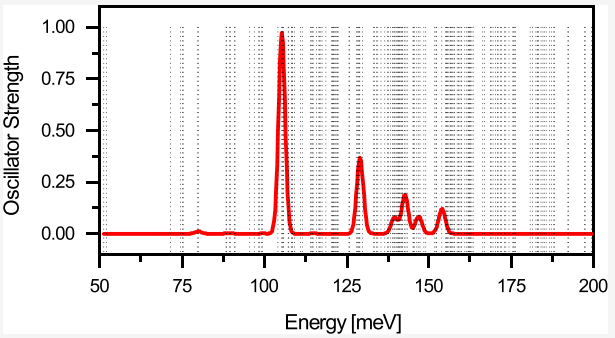

KEYWORDS: *excitons, quantum dots, graphene, two-dimensional materials, terahertz*

There is currently great interest in semiconductor quantum dots (QDs) as building blocks of quantum technology. This includes lateral gated QDs confining either spins of electrons or holes for quantum computation,[1−3] self-assembled QDs and nanoplatelets confining electrons and holes for emitters, detectors, lasers, displays, and single and entangled photon pair sources.[4−8] The gated lateral QDs allow for high tunability of their electronic properties but are limited to confining either electrons or holes, while self-assembled dots confine both electrons and holes but are difficult to tune. Simultaneously with the development of QDs in semiconductors, a new class of two-dimensional semiconductors was developed based on bilayer graphene (BLG). Optical properties of BLG were studied in the context of stage 2 intercalated graphite.[9,10] However, the isolation of a single BLG layer enables application of a vertical electric field, which opens the energy gap.[11−16] Hence, BLG turns out to be a voltage-tunable semiconductor with the energy gap in the terahertz to far infrared (FIR) range.[17]

In 2009, motivated by the tunable bandgap in BLG, Park and Louie[18] predicted the excitonic spectrum of BLG, relating the optical selection rules to Berry's phase and strong electron−hole interactions. Soon Ju et al.[14] experimentally observed excitons in BLG using photocurrent spectroscopy. They found two bright absorption peaks with the 2p exciton being the dominant bright peak, as predicted in refs 16, 18, and 19. This remarkable behavior was attributed to the pseudospin winding number of 2 found in BLG.[12,18,20,21] In 2007, Pereira et al.[22] proposed a lateral confining potential realized by position-dependent doping, confining both an electron and a hole. Furthermore, they showed that the pseudospin winding number of 2 has a dramatic effect on the angular momentum dependence of the QD spectrum, different from that of conventional semiconductors. Not only was this proposed system able to confine both electrons and holes, but it was also tunable through the use of gates. Soon several groups constructed gated lateral QDs in BLG and demonstrated confinement of either electrons or holes.[23,24] Further experimental studies of gated BLG were carried out in refs 25−27, where either confined electron or hole levels have been realized. The work on electron−electron interactions on the example of two-electron complexes was reported in refs 26, 28, and 29, where an unusual two-particle ground state, a spin-triplet but valley-singlet, was demonstrated.

In this work we establish that lateral gated QDs in BLG confine simultaneously electrons and holes. We develop a theory of such an interacting two-particle complex forming an exciton in gated BLG QDs. We start with a multimillion-atom computational box of BLG, in which we introduce vertical and lateral gates. We determine the effective lateral confining

Received: February 1, 2023
Revised: March 18, 2023
Published: March 24, 2023

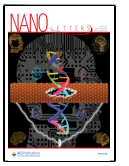

https://doi.org/10.1021/acs.nanolett.3c00406
Nano Lett. 2023, 23, 2998−3004

potential using ab-initio methods. We next compute confined QD levels in the valence and conduction band. We then calculate microscopic Coulomb interaction matrix elements,[30] the quasi-particle spectrum, and the exciton spectrum by solving the Bethe−Salpeter equation (BSE). Using excitonic states and computed dipole matrix elements, we predict the exciton fine structure and a nontrivial absorption spectrum.

We now turn to the description of BLG. We consider two Bernal-stacked layers of graphene as shown in Figure 1(a) and

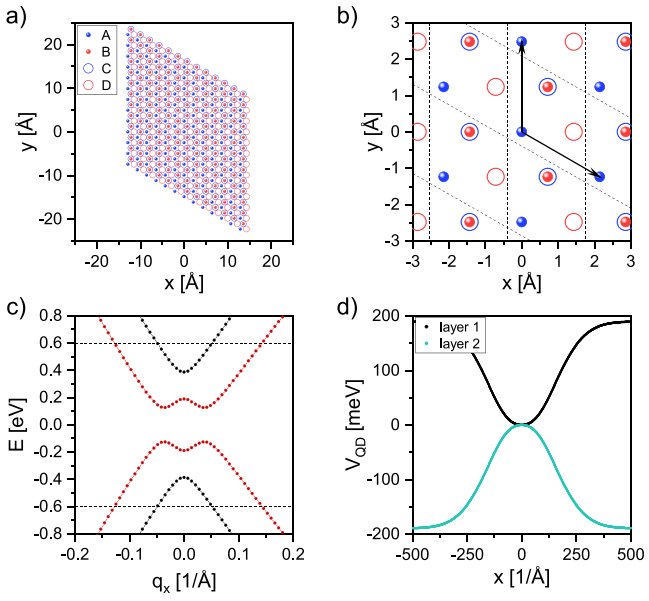

Figure 1. Model of the gated bilayer graphene system. (a) Bilayer graphene computational box. The rhomboidal geometry is not to scale. Sublattices *A*, *B* (layer 1) are shown with full symbols, while sublattices *C*, *D* (layer 2) are shown with circles. (b) A zoomed-in view of several unit cells showing the Bernal stacking. Black arrows indicate lattice vectors. (c) The bulk band structure of the bilayer graphene in the vicinity of the $\vec{K}$-point. Here, the displacement voltage is V = 0.38 eV. States within the energy window E_{cut} = 600 meV (black dotted lines) are retained in our calculations. (d) The lateral confining potential for a quantum dot with radius R_{QD} = 20 nm obtained by creating openings in the gates biasing the bilayer. The black (blue) line shows the potential on the top (bottom) layer.

(b). The sublattices are labeled *A*, *B*, *C*, *D*. We choose the real-space computational box to be rhomboidal, as shown in Figure 1(a) (drawn not to scale). Sublattices *A* and *B* belong to layer 1 while sublattices *C* and *D* compose layer 2. The nearest-neighbor in-plane bond length is a = 0.143 nm, and the distance between layers is h = 0.335 nm. The sublattice *B* on layer 1 and the sublattice *C* on layer 2 are coupled as shown in Figure 1(b), and the unit vectors are defined as $\vec{a_1} = a(0, \sqrt{3})$ and $\vec{a_2} = a\left(\frac{3}{2}, \frac{\sqrt{3}}{2}\right)$. The computational box containing our BLG structure is generated by taking $M_1 = M_2 = M$ unit cells along the $\vec{a}_1$ and $\vec{a}_2$ directions. The total number of carbon atoms in the computational box with M = 633 is 1602756. To remove the finite-size effects, we impose periodic boundary conditions connecting the opposite edges of the rhombus. We apply an external electric field (the displacement field) perpendicular to the surface. The applied voltage is $+V/2$ on layer 1 and $-V/2$ on layer 2 so that the potential difference between layers is V.

Figure 1(c) shows the band structure calculated for the intralayer tunneling matrix element $\gamma_0 = -2.5$ eV, the interlayer tunneling matrix element γ_1 = 0.34 eV, and the displacement voltage comparable to the interlayer tunneling, V = 0.38 eV. The values of γ_0 and γ_1 were obtained by fitting the tight-binding parameters to ab initio DFT calculations of the bulk BLG band structure. In the absence of the electric field,[10,31−34] the bulk BLG is gapless, but the applied electric field opens an energy gap[13,15,33,35−41] visible in Figure 1(c). At the $\vec{K}$ point of the Brillouin zone, the states corresponding to the edges of the low-energy conduction and valence bands are localized on the uncoupled sublattices *A* and *D*, respectively, with a phase difference of $2\phi_k$, which generates a Berry phase of 2π.[12,20,31−33] We also see that the opening of the gap is associated with a characteristic conduction and valence band dispersion resembling a Mexican hat, with the density of states diverging at the bottom of the conduction and top of the valence band, in analogy to one-dimensional systems.

Our goal is to confine electrons and holes laterally in BLG. This is done by removing a disc-shaped element from the top and bottom gate at the origin. Removing the circular gates lowers the potential on layer 1 from $+V/2$ to 0. This potential profile is shown in black in Figure 1(d); it confines electrons. A similar operation applied to the bottom gate that creates a potential on layer 2 which attracts holes as shown in blue in Figure 1(d). As explained in the Supporting Information, we expand the QD electronic states $\varphi_s(\vec{r})$ on the basis of band states of the computational rhombus shown in Figure 1, construct the Hamiltonian matrix on the basis of band states for the two nonequivalent valleys and spin, diagonalize it numerically, and obtain the QD energy spectrum E_s. We illustrate our results with a QD with a confining potential $\pm(V/2)e^{-\rho^2/R_{QD}^2}$ where ρ is the in-plane position of the electron and R_{QD} is the QD radius, and we take − for layer 1 and + for layer 2.

Figure 2 shows the QD energy spectrum for the QD radius R_{QD} = 20 nm for valley $\vec{K}$ near the Fermi level set at zero. We see that the confinement of electrons and holes results in the reduction of the single-particle energy gap, 380 meV in the bulk, to ∼40 meV. We find the QD energy spectrum to be very

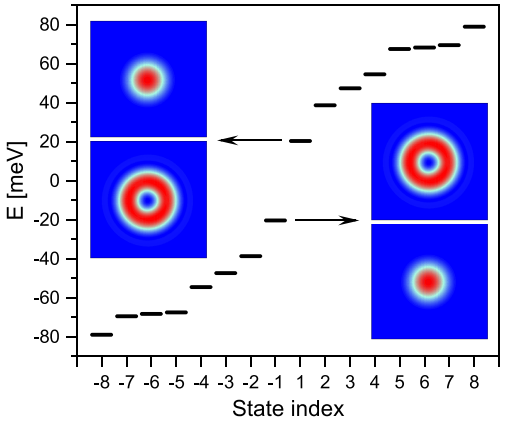

Figure 2. Single-particle energy spectrum of the quantum dot. Single-particle energy levels of the gated bilayer graphene quantum dot as a function of level index for the $-\vec{K}$ valley. Inset shows the probability densities corresponding to the level −1 (top of the valence band) and level +1 (bottom of the conduction band). Here, upper (lower) plots show the probability density on the top (bottom) layer.

https://doi.org/10.1021/acs.nanolett.3c00406
Nano Lett. 2023, 23, 2998−3004

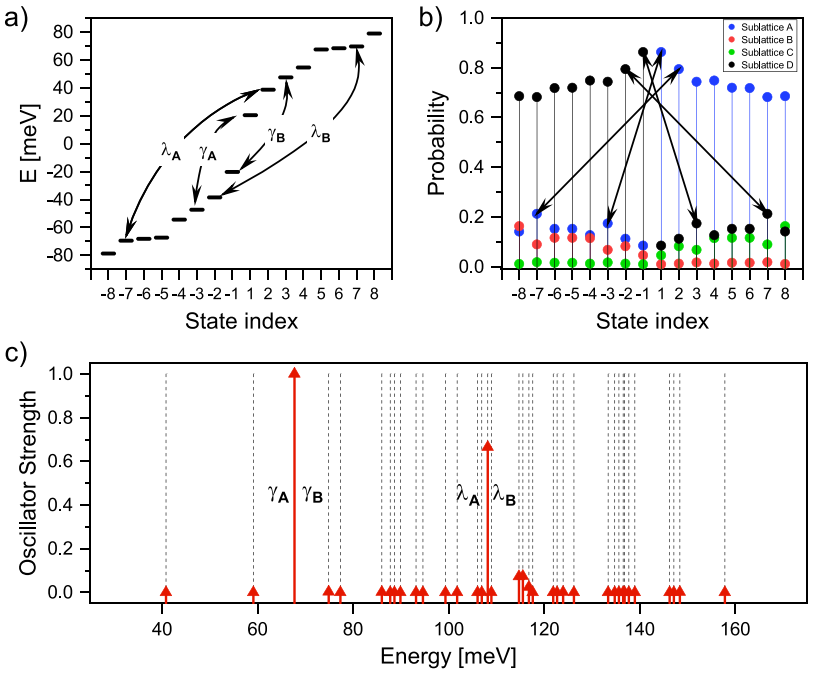

Figure 3. Dipole moments for optical transitions. (a) The quantum dot energy spectrum equivalent to that from Figure 2. Arrows connect the pairs of valence and conduction states connected by nonzero dipole elements, indicating contributions to the absorption spectrum. (b) Charge density of the single-particle wave functions decomposed into sublattices of the bilayer graphene. For each state labeled by the state index (horizontal axis), its charge density portion from sublattices A, B, C, and D is indicated respectively by the blue, red, green, and black lines and symbols. The black arrows indicate pairs of states (one from the valence band and one from the conduction band) connected by large dipole matrix elements. (c) Joint optical density of states for the noninteracting electron and hole in the bilayer graphene quantum dot. Dashed lines indicate the energy gaps between the valence and conduction single-particle levels, while red arrows show the magnitude (absolute value squared) of the corresponding dipole elements calculated for states from the valley $-\vec{K}$.

different from that found in gated lateral QD in GaAs or self-assembled QDs, which are understood in terms of electronic shells of a two-dimensional harmonic oscillator.[42−44] The insets in Figure 2 show the electronic wave functions on layer 1 (top) and layer 2 (bottom) for states at the top of the valence band and at the bottom of the conduction band. We see that the lowest of the conduction-band states is s-like, followed by two levels of a p shell which is split in energy. The splitting is due to topology and the emergence of a winding number of 2 in BLG near the K-point and is well discussed in ref 22. However, the next group of levels cannot be understood in terms of the three levels of a d shell. Hence, the single-particle spectrum here is different from self-assembled and gated QDs, even for different radii of the confining potential, as pointed out by Peeters and co-workers.[22]

Figure 3 shows the effect of the wave functions on dipole matrix elements controlling the coupling of the QD with light. As explained in the Supporting Information, we computed dipole matrix elements $\vec{D}_{s,s'} = \langle s|\vec{r}|s'\rangle$ connecting QD states s and s'. The arrows in Figure 3(a) show which states in the valence band are connected with which states in the conduction band by finite dipole matrix elements. We see that, unlike in self-assembled quantum dots, the state at the top of the valence band (number −1) is not connected with the lowest-energy state (number +1) in the conduction band, but with the third excited state (number +3). By symmetry, the state at the bottom of the conduction band (number +1) is connected with the valence band state number −3. The second-highest in energy valence band state (number −2) is now connected with the highly excited conduction band state number +7. Figure 3(b) shows how the probability density corresponding to different states is distributed over sublattices. In particular, we see that the large dipole elements correspond to the two QD states residing largely on the same sublattice. For example, state number +3 and state number −1 both occupy the sublattice B. As we shall show, this complicated light−matter coupling is further significantly modified by electron−electron interactions.

We start our many-body analysis by approximating the many-electron ground state as a single Slater determinant $|GS\rangle = \prod_{p,\sigma} c^{\dagger}_{p\sigma}|0\rangle$ of all occupied valley and spin QD valence band states shown in Figure 2. Here, $c^{\dagger}_{p\sigma}$ creates an electron with spin σ in a p state of the valence band. Next, we write the exciton states $|\psi^{\mu}\rangle$ as a linear combination of one electron−hole pair excitations conserving S_z as

$$|\psi^{\mu}\rangle = \sum_{p,q,\sigma} A^{\mu}_{p,q,\sigma} c^{\dagger}_{q\sigma} c_{p\sigma}|GS\rangle \tag{1}$$

Here $A^{\mu}_{p,q,\sigma}$ is the amplitude of the electron−hole pair, where $c_{p\sigma}$ removes an electron with spin σ from the valence band state p, leaving behind a hole, and $c^{\dagger}_{q\sigma}$ places this electron in the empty conduction band state q. The index p runs over all valence band states, and the index q goes through all unoccupied conduction band states of the QD. Different electron−hole pair excitations are coupled by the electron−electron interaction V_C (for details see the Supporting Information), which renormalizes the exciton energy. The amplitudes $A^{\mu}_{p,q,\sigma}$ of the electron−hole pairs satisfy the BSE:

https://doi.org/10.1021/acs.nanolett.3c00406
Nano Lett. 2023, 23, 2998−3004

$$\sum_{q',p',\sigma'} [(E_{q',\sigma'} + \Sigma_{q',\sigma'}) - (E_{p',\sigma'} + \Sigma_{p',\sigma'})]\delta_{p,p'}\delta_{q,q}\delta_{\sigma,\sigma'}A^{\mu}_{p',q',\sigma'} + \sum_{q',p',\sigma'} [\langle p, q'|V_C|p', q\rangle - \langle p, q'|V_C|q, p'\rangle\delta_{\sigma\sigma'}]A^{\mu}_{p',q',\sigma'} = E_{\mu}A^{\mu}_{p,q,\sigma} \quad (2)$$

Here, the electron−hole pair energy is renormalized by the self-energy, which in the screened Hartree−Fock approximation is given by $\Sigma_{p,\sigma} = -\sum_{q,\sigma'}\delta_{\sigma,\sigma'}\langle q,p|V_C|q,p\rangle$, where the sum over q runs over the valence band states. In this example of a QD, we find self-energies at the top of the valence band and at the bottom of the conduction band to converge with 120 filled valence band QD states. The scattering of electron−hole pairs (the vertex correction) is controlled by an attractive (negative) direct term and a repulsive (positive) exchange term. We note that the BSE for a QD contains all possible electron−hole pairs, accounting for the mixing of the relative and center of mass motion.

To compute the excitonic states, we solve the BSE given above in the subspace of 32 single-particle states near the Fermi level. These states are shown for one valley in Figure 2. These states give the most important contribution to the low-energy exciton spectra. We start our analysis by computing the spectrum of noninteracting electron−hole pairs, i.e., $V_C \equiv 0$, shown in Figure 4(a). We find degenerate shells of electron−hole levels, forming either 8-fold or 16-fold degenerate manifolds. The 8-fold degeneracy can be understood by constructing all electron−hole pairs that have the energy of the single-particle energy gap and conserve total S_z. This corresponds to removing an electron from state number −1 and placing it on state number +1 in Figure 4(a). Both states −1 and +1 have spin and valley degeneracy. There will be two electron−hole pairs in each valley (total of four, including spin) and four more between valleys. Thus, we have eight possible electron−hole pairs with the energy of the single-particle gap. To understand the 16-fold manifold, let us consider the second lowest-energy electron−hole pairs. These pairs are constructed by exciting electrons from state −1 to state +2 and from state −2 to state +1 in Figure 2(a). The two possibilities arising from the electron−hole symmetry double the resulting degeneracy to 16.

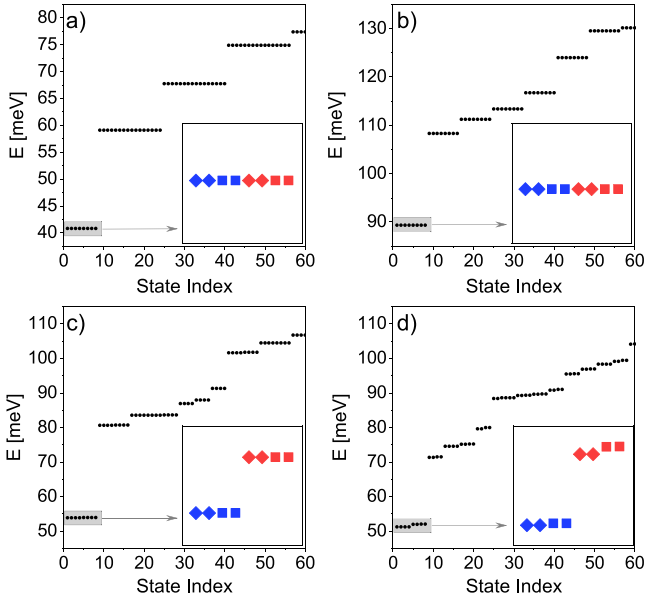

Figure 4. Excitonic energy spectra in different stages of including Coulomb interactions. (a) Energies of noninteracting electron−hole pairs. (b) Energy spectrum of the pairs renormalized by self-energies. (c) Energy spectrum of the pairs accounting for the self-energies and vertex corrections (the electron−hole attraction) but without correlations. (d) Excitonic energy diagram accounting for all aspects of the electron−electron interaction. The boxes in the bottom right of each figure show the 8 lowest energy states zoomed in. The states are labeled as intervalley (blue), intravalley (red), singlet (squares), and triplets (diamonds).

Next, we turn on the self-energy contribution to the electron−hole pair energies. The resulting spectrum is shown in Figure 4(b). The self-energies result in a large blue shift of the electron−hole pair energies. Furthermore, the self-energies split the 16-fold degenerate manifolds into two subclasses because the values of the self-energy in the excitations involving states −1 and +2 are different than those involving states −2 and +1. We next calculate the energies of electron−hole pairs including self-energies and vertex corrections, i.e., the electron−hole attraction. These spectra are shown in Figure 4(c). Direct electron−hole attraction is large and lowers the energy of the electron−hole complex, while the electron−hole exchange interaction is repulsive and raises the energy of the complex slightly. While the direct electron−hole interaction does not discriminate valleys, the exchange interaction is different within a valley and between valleys. This separates the energy of intervalley and intravalley electron−hole pairs. Indeed, the intervalley electron−hole pair has a lower energy due to its smaller repulsive exchange interaction. We also observe reordering higher-energy electron−hole pairs due to large exchange values compared to the single-particle level spacing.

Finally, we include the Coulomb scattering connecting electron−hole pairs and solve the full BSE. The resulting excitonic spectrum is shown in Figure 4(d). The single-particle gap is 40 meV, the gap which is renormalized by self-energies is 90 meV, and the exciton energy is 50 meV. Hence, the exciton binding energy is positive. The excitonic states can be categorized as inter/intravalley singlets/triplets. The insets in Figure 4 categorize the low-energy states accordingly. The intervalley excitons are at lower energies than their intravalley counterparts because the repulsive exchange interaction for intravalley excitons is stronger. Furthermore, each class of intravalley and intervalley excitons is further split into spin singlet and triplets. Triplets are at lower energies than their singlet counterparts as the exchange now favors the triplets in energy. Focusing on the ground state, we see that it is approximately 4-fold degenerate and corresponds to intervalley excitons formed from electron−hole pairs across the gap. The singlet−triplet splitting for these states is negligible and is the reason why it appears 4-fold rather than 2-fold degenerate.

We now proceed to computing the absorption spectrum $A(\omega)$ as a function of the photon energy ω:

$$A(\omega) = \sum_{\mu} \left| \sum_{s,s',\sigma} \mathcal{E}_0^{\pm}\cdot\vec{D}_{s,s'}(A^{\mu}_{s,s',\sigma})^* \right|^2 \delta(E_{\mu} - \omega) \quad (3)$$

Here, $\mathcal{E}_0^{\pm}$ is the polarization vector for the incident photon, represented by a circularly polarized electric field, and $\vec{D}_{s,s'}$ are dipole matrix elements. Figure 5 shows the absorption spectrum as a function of the photon energy for our model

https://doi.org/10.1021/acs.nanolett.3c00406
Nano Lett. 2023, 23, 2998−3004

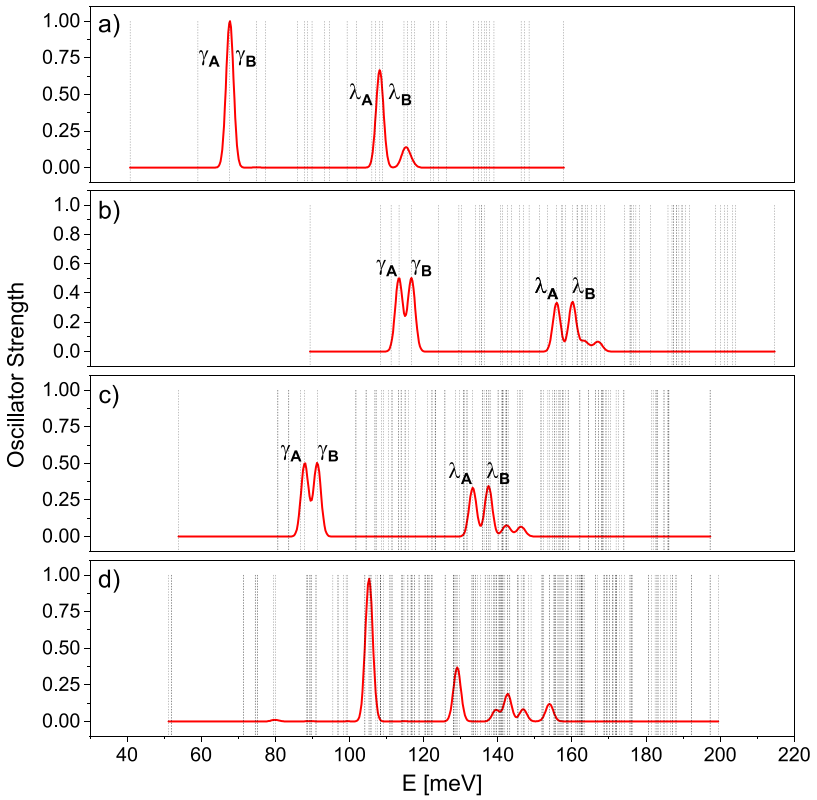

Figure 5. Excitonic absorption spectra. Absorption spectrum of the gated lateral bilayer graphene quantum dot as a function of the photon energy (horizontal axis) in different stages of including Coulomb interactions. (a) Noninteracting electron−hole pairs. (b) Self-energies are included. (c) Self-energies and vertex corrections (electron−hole attraction) are included. (d) Self-energies, vertex corrections, and correlation effects are included. Black dashed lines correspond to energies of the excitonic states shown in corresponding panels of Figure 4, while the red line shows the absorption spectrum computed from the Fermi's Golden Rule.

QD. The vertical black lines correspond to energies E_μ of excitonic states, while the red line corresponds to excitonic states contributing to absorption. In Figure 5(a) we show the absorption spectrum ignoring interactions. We find the low-energy electron−hole pairs to be dark. This is a consequence of the previously discussed zero dipole matrix elements for the two lowest-energy electron−hole complexes. The third dashed line corresponds to the first bright peak at around 67 meV. This is the energy of the e−h pair with a large dipole matrix element, i.e., the 16-fold degenerate third manifold shown in Figure 4(a). A second smaller peak is seen in Figure 5(a) at around 108 meV. This maximum corresponds to the second bright dipole matrix element shown in Figure 3(c).

We now turn on the effects of self-energies shown in Figure 5(b). As already discussed, self-energies split the 16-fold manifold into two submanifolds, and thus the single large peak which was composed of the transitions γ_A and γ_B labeled in Figure 3 has split into two. The peaks have also shifted to higher energies due to the blue shift introduced by the self-energies.

The inclusion of the electron−hole attraction causes a red shift shown in Figure 5(c), bringing the absorption maxima closer in energy to the noninteracting peaks. The vertex correction has also broken the degeneracy of intravalley and intervalley electron−hole pairs. Reordering of levels occurs due to the electron−hole exchange, and new dark states emerge at an energy lower than that of the bright state.

Finally, when the scattering terms are accounted for in the full BSE, the degenerate states split into triplets and singlets, with triplets being dark, as shown in Figure 5(d). The lowest exciton energy decreased to 50 meV due to correlations, but the bright exciton peak has moved to higher energy due to the singlet−triplet splitting. Many new dark states emerge at low energies since the dark triplets have shifted down in energy. More level reordering occurred due to the singlet triplet splitting as well as correlations. The bright peak is now blue shifted to 110 meV, i.e., ∼30 Thz. There is a second smaller peak at 130 meV which corresponds to the second optically active transition. This transition is smeared out in the interacting system since correlations spread the relevant optically active electron−hole pairs among many exciton states. The many dark low-energy excitonic states are either intervalley excitons or spin triplets or have vanishing dipole matrix elements. The presence of many low-energy dark states makes these BLG QDs potential candidates for storage of photons.

In summary, we developed a theory of excitons confined in laterally gated bilayer graphene quantum dots. These nanostructures combine the ability to confine electrons and holes of semiconductor self-assembled quantum dots with the tunability of laterally gated semiconductor quantum dots, with the latter confining only either electrons or holes. Here we describe such a strongly interacting electron−hole complex forming an electrically tunable exciton. We find these excitons to be very different from excitons found in semiconductor quantum dots and nanocrystals. Indeed, the exciton energy as well as the absorption and emission spectrum is tunable by voltage from the terahertz to FIR range. The conservation of

https://doi.org/10.1021/acs.nanolett.3c00406
Nano Lett. 2023, 23, 2998−3004

spin, valley, and orbital angular momentum results in a band of dark low-energy states making this system a promising candidate for storage, detection, and emission of photons in the terahertz range.

■ ASSOCIATED CONTENT

Supporting Information

The Supporting Information is available free of charge at https://pubs.acs.org/doi/10.1021/acs.nanolett.3c00406.

Additional information on the theoretical model including: obtaining the single-particle energies and wave functions, details on obtaining and solving the Bethe−Salpeter equation, and details on obtaining dipole matrix elements and computing absorption (PDF)

■ AUTHOR INFORMATION

Corresponding Author

Yasser Saleem − *Department of Physics, University of Ottawa, Ottawa K1N6N5, Canada;* orcid.org/0000-0002-9061-6110; Email: yassersaleem461@gmail.com

Authors

Katarzyna Sadecka − *Department of Physics, University of Ottawa, Ottawa K1N6N5, Canada; Institute of Theoretical Physics, Wrocław University of Science and Technology, 50-370 Wrocław, Poland*

Marek Korkusinski − *Department of Physics, University of Ottawa, Ottawa K1N6N5, Canada; Security and Disruptive Technologies, National Research Council, Ottawa K1A0R6, Canada*

Daniel Miravet − *Department of Physics, University of Ottawa, Ottawa K1N6N5, Canada*

Amintor Dusko − *Department of Physics, University of Ottawa, Ottawa K1N6N5, Canada*

Pawel Hawrylak − *Department of Physics, University of Ottawa, Ottawa K1N6N5, Canada*

Complete contact information is available at: https://pubs.acs.org/10.1021/acs.nanolett.3c00406

Notes

The authors declare no competing financial interest.

■ ACKNOWLEDGMENTS

This research was supported by NSERC QC2DM Strategic Grant No. STPG-521420, NSERC Discovery Grant No. RGPIN2019-05714, NRC QSP 078 project, University of Ottawa Research Chair in Quantum Theory of Materials, Nanostructures, and Devices and Digital Research Alliance Canada with computing resources. Y.S. and K.S. are thankful for financial support from the Polish National Agency for Academic Exchange (NAWA), Poland, grant PPI/APM/2019/1/00085/U/00001.

■ REFERENCES

(1) Ciorga, M.; Sachrajda, A. S.; Hawrylak, P.; Gould, C.; Zawadzki, P.; Jullian, S.; Feng, Y.; Wasilewski, Z. Addition spectrum of a lateral dot from Coulomb and spin-blockade spectroscopy. *Phys. Rev. B* **2000**, *61*, R16315.

(2) Hsieh, C.-Y.; Shim, Y.-P.; Korkusinski, M.; Hawrylak, P. Physics of lateral triple quantum-dot molecules with controlled electron numbers. *Rep. Prog. Phys.* **2012**, *75*, 114501.

(3) Burkard, G.; Ladd, T. D.; Nichol, J. M.; Pan, A.; Petta, J. R. Semiconductor spin qubits. *arXiv.org/2112.08863*, 2021; https://arxiv.org/abs/2112.08863 (accessed March 15, 2023).

(4) García de Arquer, F. P.; Talapin, D. V.; Klimov, V. I.; Arakawa, Y.; Bayer, M.; Sargent, E. H. Semiconductor quantum dots: Technological progress and future challenges. *Science* **2021**, *373*, aaz8541.

(5) Bayer, M.; Stern, O.; Hawrylak, P.; Fafard, S.; Forchel, A. Hidden symmetries in the energy levels of excitonic 'artificial atoms'. *Nature* **2000**, *405*, 923−926.

(6) Hawrylak, P.; Narvaez, G. A.; Bayer, M.; Forchel, A. Excitonic absorption in a quantum dot. *Phys. Rev. Lett.* **2000**, *85*, 389.

(7) Schwartz, I.; Cogan, D.; Schmidgall, E. R.; Don, Y.; Gantz, L.; Kenneth, O.; Lindner, N. H.; Gershoni, D. Deterministic generation of a cluster state of entangled photons. *Science* **2016**, *354*, 434−437.

(8) Laferrière, P.; Yeung, E.; Korkusinski, M.; Poole, P. J.; Williams, R. L.; Dalacu, D.; Manalo, J.; Cygorek, M.; Altintas, A.; Hawrylak, P. Systematic study of the emission spectra of nanowire quantum dots. *Appl. Phys. Lett.* **2021**, *118*, 161107.

(9) Blinowski, J.; Hau, N. H.; Rigaux, C.; Vieren, J. P.; Le Toullec, R.; Furdin, G.; Hérold, A.; Melin, J. Band structure model and dynamical dielectric function in lowest stages of graphite acceptor compounds. *J. Phys. France* **1980**, *41*, 47−58.

(10) Hoffman, D.; Eklund, P.; Heinz, R.; Hawrylak, P.; Subbaswamy, K. Effect of c axis dispersion on the optical properties of acceptor graphite intercalation compounds. *Phys. Rev. B* **1985**, *31*, 3973.

(11) Zhang, L. M.; Li, Z. Q.; Basov, D. N.; Fogler, M. M.; Hao, Z.; Martin, M. C. Determination of the electronic structure of bilayer graphene from infrared spectroscopy. *Phys. Rev. B* **2008**, *78*, 235408.

(12) Novoselov, K. S.; McCann, E.; Morozov, S. V.; Fal'ko, V. I.; Katsnelson, M. I.; Zeitler, U.; Jiang, D.; Schedin, F.; Geim, A. K. Unconventional quantum Hall effect and Berry's phase of 2π in bilayer graphene. *Nat. Phys.* **2006**, *2*, 177−180.

(13) Zhang, Y.; Tang, T. T.; Girit, C.; Hao, Z.; Martin, M. C.; Zettl, A.; Crommie, M. F.; Ron Shen, Y.; Wang, F. Direct observation of a widely tunable bandgap in bilayer graphene. *Nature* **2009**, *459*, 820−823.

(14) Ju, L.; Wang, L.; Cao, T.; Taniguchi, T.; Watanabe, K.; Louie, S. G.; Rana, F.; Park, J.; Hone, J.; Wang, F.; McEuen, P. L. Tunable excitons in bilayer graphene. *Science* **2017**, *358*, 907−910.

(15) Castro, E. V.; Novoselov, K. S.; Morozov, S. V.; Peres, N. M. R.; Dos Santos, J. L.; Nilsson, J.; Guinea, F.; Geim, A. K.; Neto, A. C. Biased Bilayer Graphene: Semiconductor with a Gap Tunable by the Electric Field Effect. *Phys. Rev. Lett.* **2007**, *99*, 216802.

(16) Sauer, M.; Pedersen, T. Exciton absorption, band structure, and optical emission in biased bilayer graphene. *Phys. Rev. B* **2022**, *105*, 115416.

(17) Bandurin, D. A.; Svintsov, D.; Gayduchenko, I.; Xu, S. G.; Principi, A.; Moskotin, M.; Tretyakov, I.; Yagodkin, D.; Zhukov, S.; Taniguchi, T.; Watanabe, K.; Grigorieva, I. V.; Polini, M.; Goltsman, G. N.; Geim, A. K.; Fedorov, G. Resonant terahertz detection using graphene plasmons. *Nature Commun.* **2018**, *9*, 5392.

(18) Park, C.-H.; Louie, S. G. Tunable Excitons in Biased Bilayer Graphene. *Nano Lett.* **2010**, *10*, 426−431.

(19) Henriques, J. C. G.; Epstein, I.; Peres, N. M. R. Absorption and optical selection rules of tunable excitons in biased bilayer graphene. *Phys. Rev. B* **2022**, *105*, 045411.

(20) Park, C.-H.; Marzari, N. Berry phase and pseudospin winding number in bilayer graphene. *Phys. Rev. B* **2011**, *84*, 205440.

(21) Zhang, F.; Jung, J.; Fiete, G. A.; Niu, Q.; MacDonald, A. H. Spontaneous quantum Hall states in chirally stacked few-layer graphene systems. *Phys. Rev. Lett.* **2011**, *106*, 156801.

(22) Pereira, J. M.; Vasilopoulos, P.; Peeters, F. M. Tunable quantum dots in bilayer graphene. *Nano Lett.* **2007**, *7*, 946−949.

(23) Eich, M.; Herman, F.; Pisoni, R.; Overweg, H.; Kurzmann, A.; Lee, Y.; Rickhaus, P.; Watanabe, K.; Taniguchi, T.; Sigrist, M.; Ihn, T.; Ensslin, K. Spin and valley states in gate-defined bilayer graphene quantum dots. *Phys. Rev. X* **2018**, *8*, 031023.

(24) Banszerus, L.; Rothstein, A.; Fabian, T.; Moller, S.; Icking, E.; Trellenkamp, S.; Lentz, F.; Neumaier, D.; Watanabe, K.; Taniguchi, T.; Libisch, F.; Volk, C.; Stampfer, C. Electron-hole crossover in gate-controlled bilayer graphene quantum dots. *Nano Lett.* **2020**, *20*, 7709−7715.
(25) Kurzmann, A.; Overweg, H.; Eich, M.; Pally, A.; Rickhaus, P.; Pisoni, R.; Lee, Y.; Watanabe, K.; Taniguchi, T.; Ihn, T.; Ensslin, K. Charge detection in gate-defined bilayer graphene quantum dots. *Nano Lett.* **2019**, *19*, 5216−5221.
(26) Kurzmann, A.; Eich, M.; Overweg, H.; Mangold, M.; Herman, F.; Rickhaus, P.; Pisoni, R.; Lee, Y.; Garreis, R.; Tong, C.; Watanabe, K.; Taniguchi, T.; Ensslin, K.; Ihn, T. Excited states in bilayer graphene quantum dots. *Phys. Rev. Lett.* **2019**, *123*, 026803.
(27) Banszerus, L.; Möller, L.; Steiner, S.; Icking, C.; Trellenkamp, S.; Lentz, F.; Watanabe, K.; Taniguchi, T.; Volk, C.; Stampfer, C. Spin-valley coupling in single-electron bilayer graphene quantum dots. *Nature Commun.* **2021**, *12*, 5250.
(28) Zarenia, M.; Partoens, B.; Chakraborty, T.; Peeters, F. M. Electron-electron interactions in bilayer graphene quantum dots. *Phys. Rev. B* **2013**, *88*, 245432.
(29) Korkusinski, M.; Saleem, Y.; Miravet, D.; Dusko, A.; Hawrylak, P. Spontaneously broken spin and valley states in bilayer graphene quantum dots. To be published.
(30) Kotov, V. N.; Uchoa, B.; Pereira, V. M.; Guinea, F.; Neto, A. C. Electron-electron interactions in graphene: Current status and perspectives. *Rev. Mod. Phys.* **2012**, *84*, 1067.
(31) McCann, E.; Fal'ko, V. I. Landau-level degeneracy and quantum hall effect in a graphite bilayer. *Phys. Rev. Lett.* **2006**, *96*, 086805.
(32) McCann, E.; Abergel, D. S.; Fal'ko, V. I. The low energy electronic band structure of bilayer graphene. *Eur. Phys. J. Special Topics* **2007**, *148*, 91−103.
(33) McCann, E.; Koshino, M. The electronic properties of bilayer graphene. *Rep. Prog. Phys.* **2013**, *76*, 056503.
(34) Leaw, J. N.; Tang, H. K.; Sengupta, P.; Assaad, F. F.; Herbut, I. F.; Adam, S. Electronic ground state in bilayer graphene with realistic coulomb interactions. *Phys. Rev. B* **2019**, *100*, 125116.
(35) Wang, F.; Zhang, Y.; Tian, C.; Girit, C.; Zettl, A.; Crommie, M.; Shen, Y. R. Gate-Variable Optical Transitions in Graphene. *Science* **2008**, *320*, 206−209.
(36) Min, H.; Sahu, B.; Banerjee, S. K.; MacDonald, A. H. Ab initio theory of gate induced gaps in graphene bilayers. *Phys. Rev. B* **2007**, *75*, 155115.
(37) Aoki, M.; Amawashi, H. Dependence of band structures on stacking and field in layered graphene. *Solid State Commun.* **2007**, *142*, 123−127.
(38) Gava, P.; Lazzeri, M.; Saitta, A. M.; Mauri, F. Ab initio study of gap opening and screening effects in gated bilayer graphene. *Phys. Rev. B* **2009**, *79*, 165431.
(39) Falkovsky, L. A. Gate-tunable bandgap in bilayer graphene. *J. Experim. Theor. Phys.* **2010**, *110*, 319−324.
(40) Ohta, T.; Bostwick, A.; Seyller, T.; Horn, K.; Rotenberg, E. Controlling the Electronic Structure of Bilayer Graphene. *Science* **2006**, *313*, 951−954.
(41) Mak, K. F.; Lui, C. H.; Shan, J.; Heinz, T. F. Observation of an Electric-Field-Induced Band Gap in Bilayer Graphene by Infrared Spectroscopy. *Phys. Rev. Lett.* **2009**, *102*, 256405.
(42) Hawrylak, P. Single-electron capacitance spectroscopy of few-electron artificial atoms in a magnetic field: Theory and experiment. *Phys. Rev. Lett.* **1993**, *71*, 3347.
(43) Raymond, S.; Studenikin, S.; Sachrajda, A.; Wasilewski, Z.; Cheng, S. J.; Sheng, W.; Hawrylak, P.; Babinski, A.; Potemski, M.; Ortner, G.; Bayer, M. Excitonic energy shell structure of self-assembled InGaAs/GaAs quantum dots. *Phys. Rev. Lett.* **2004**, *92*, 187402.
(44) Gomes, J.; Vasilevskiy, M. Variational calculation of the lowest exciton states in phosphorene and transition metal dichalcogenides. *J. Phys.: Condens. Matter* **2022**, *34*, 045702.

https://doi.org/10.1021/acs.nanolett.3c00406
Nano Lett. 2023, 23, 2998−3004